JACS Au
AN OPEN ACCESS JOURNAL OF THE AMERICAN CHEMICAL SOCIETY

pubs.acs.org/jacsau

Article

CO Adsorbate Promotes Polaron Photoactivity on the Reduced Rutile TiO_2(110) Surface

Cheng Cheng, Yonghao Zhu, Wei-Hai Fang, Run Long,* and Oleg V. Prezhdo

Cite This: *JACS Au* 2022, 2, 234–245

Read Online

ACCESS | Metrics & More | Article Recommendations | Supporting Information

ABSTRACT: Polarons play a major role in determining the chemical properties of transition-metal oxides. Recent experiments show that adsorbates can attract inner polarons to surface sites. These findings require an atomistic understanding of the adsorbate influence on polaron dynamics and lifetime. We consider reduced rutile TiO_2(110) with an oxygen vacancy as a prototypical surface and a CO molecule as a classic probe and perform *ab initio* adiabatic molecular dynamics, time-domain density functional theory, and nonadiabatic molecular dynamics simulations. The simulations show that subsurface polarons have little influence on CO adsorption and CO can desorb easily. On the contrary, surface polarons strongly enhance CO adsorption. At the same time, the adsorbed CO attracts polarons to the surface, allowing them to participate in catalytic processes with CO. The CO interaction with polarons changes their orbital origin, suppresses polaron hopping, and stabilizes them at surface sites. Partial delocalization of polarons onto CO decouples them from free holes, decreasing the nonadiabatic coupling and shortening the quantum coherence time, thereby reducing charge recombination. The calculations demonstrate that CO prefers to adsorb at the next-nearest-neighbor five-coordinated Ti^{3+} surface electron polaron sites. The reported results provide a fundamental understanding of the influence of electron polarons on the initial stage of reactant adsorption and the effect of the adsorbate–polaron interaction on the polaron dynamics and lifetime. The study demonstrates how charge and polaron properties can be controlled by adsorbed species, allowing one to design high-performance transition-metal oxide catalysts.

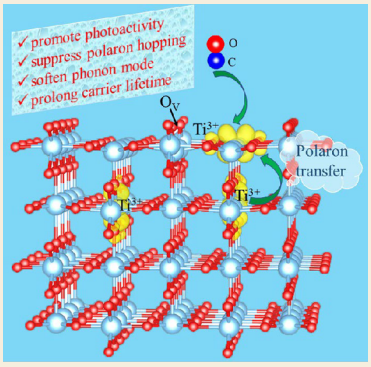

KEYWORDS: *TiO_2, polaron, adsorbate–polaron interaction, electron–hole recombination, nonadiabatic molecular dynamics, time-dependent density functional theory*

1. INTRODUCTION

Transition-metal oxides (TMOs) are receiving worldwide attention as one of the most promising classes of semiconductors for photoelectrochemical energy conversion.[1−4] Formation of electron polarons (EPs) in TMOs by excess electrons, introduced by intrinsic defects,[5,6] doping,[7,8] interstitials,[9,10] and light irradiation,[11] is an intrinsic and pervasive phenomenon that has strong impact on surface chemistry. EPs are formed by a local distortion of the lattice that creates a self-trapping potential for the charge carrier. Such self-trapping strongly changes material's charge carrier mobility and chemical reactivity.[12] Surface oxygen vacancies (O_V) are regarded to be particularly reactive, contributing to the versatile chemical processes in TMOs.[13−15] A surface O_V gives rise to two small EPs with energy levels deep inside the bandgap, depending on electron–phonon coupling in various TMOs.[16−19] Even a small thermal energy can activate EPs to hop to different lattice sites, modifying properties of the polaronic states and creating challenges in understanding of the nonequilibrium dynamics of polarons.[20] There are debates in the literature on whether polarons promote carrier conductivity[21−23] or behave as deep carrier recombination centers that are detrimental to conductivity.[24,25] Deeper lying polarons tend to redistribute toward the surface and can facilitate efficient charge transfer to catalytic sites, driving various chemical reaction processes. Understanding how adsorbates influence polaron behavior is of fundamental importance for TMO catalytic properties and rational design of high-performance photocatalysts.[26]

In recent years, many experimental and theoretical works aimed to elucidate the mechanisms underlying high catalytic reactivity of TMOs and involving interactions between polarons and adsorbed species. These works suggested that adsorbates could influence polaron stability and redistribute polarons to surface sites. Simultaneously, reactant binding energy and efficiency of reactant dissociation can be enhanced.[10,27−30] Density functional theory (DFT) calculations conducted by the Liu group reported that EPs induced by titanium interstitials or single hydrogen atom preferred to

Received: November 9, 2021
Published: December 30, 2021

https://doi.org/10.1021/jacsau.1c00508
JACS Au 2022, 2, 234–245

reside in deeper inner layers when the surface was clean, while they tended to diffuse toward surface sites in the presence of adsorbed water or methanol.[9,30] The polaron−adsorbate interaction drove partial dissociations of the adsorbates on the reduced TiO_2(110) surface. Resonant photoelectron diffraction measurements verified that these small polarons preferentially distributed in the subsurface of rutile TiO_2(110).[5,7] Subsurface polarons are not chemically active and need to migrate to the surface to participate in chemical reactions. This is achieved typically by increasing temperature to overcome energy barrier and unfavorable driving force. Instead of raising temperature, adsorbed molecules, such as CO, can be used to bias EPs toward the surface. These adsorbates do not necessarily participate in the photocatalytic process of interest, but attract polarons to the surface without using them up. In turn, polaron migration toward the surface can enhance adsorption of such helper molecules, while polaron consumption by other species participating in photochemical reactions can weaken the helper molecule binding. Scanning tunneling microscopy (STM) and photoemission experiments verified the H_2O-induced surface aggregation of polarons in TiO_2(110), related to the subsequent catalytic activity.[29] Using UV photoemission spectroscopy, two-photon photoemission spectroscopy and DFT, Tanner et al. demonstrated that carboxylate adsorption promoted polaron redistribution toward the surface by adsorbate coupling with the polaronic states.[28] By combining STM measurements with DFT calculations, Reticcioli et al. found that adsorbed CO showed attractive coupling with polarons and induced diffusion of subsurface EPs toward the rutile TiO_2(110) surface.[10] The strong coupling between CO and polarons altered the CO adsorption and affected polaron stability, which may explain the substantially increased CO photo-oxidation reactivity. Likewise, by combining IR spectroscopy and DFT calculations, Cao et al. suggested transformation of sublayer polarons into surface polarons, induced by adsorption of CO and NO molecules.[27] A combined experimental/theoretical study of CO adsorbed on Ti-containing materials showed a complex photochemistry involving plasmons and polaronic effects.[31]

Further studies are needed in order to understand more thoroughly the interactions between adsorbates, polarons, and active catalytic sites and to reconcile conflicting results. For example, the STM studies of CO adsorption sites on reduced TiO_2(110) indicated that CO tends to adsorb at the next-nearest-neighbor five-coordinated Ti sites (NNN-Ti_{5c}) relative to O_V.[32] On the other hand, DFT calculations showed that the energy of adsorption of CO at O_V was higher by 0.01−0.15 eV than that at the NNN-Ti_{5c} site.[33,34] Reticcioli et al. argued that CO-induced polaron diffusion from the subsurface to the surface NNN-Ti_{5c} sites and strong CO-polaron interactions changed the CO adsorption energy.[10] The limitations of the experimental setups and the static DFT calculations corresponding to 0 K motivate more realistic calculations at finite temperatures, including both atom and electron dynamics. Knowledge of evolving local geometric and electronic structure and quantum dynamics of coupled polarons, charges, and phonons is essential for understanding and controlling the adsorption and catalytic properties of TMOs. It is important to know whether localization of polarons on the surface by interaction with CO molecules changes polaron lifetime and what factors cause such changes. One can expect that CO and other light molecules accelerate polaron recombination, since they have high frequency vibrations that can accommodate the excess electronic energy released during the relaxation more easily than the slower TiO_2 phonons. It is also possible that polarons located on the surface hop via nonadiabatic (NA) transitions to polaron states located in subsurface. If polaron state energies, hopping, and recombination are related to properties of the adsorbed molecules, then one can tune both polaron chemical activity and lifetimes by molecule choice.

In this work, we use the rutile TiO_2(110) surface containing an O_V and a CO molecule as a classic photocatalytic system to probe the interaction of EPs and adsorbates. Although experiments have demonstrated that defective rutile TiO_2(110) with adsorbed CO exhibits good photocatalytic activity,[32,34,35] the dynamics of coupled CO and EPs have not been fully established. Such analysis is challenging for the following reasons. First, the effect of EPs on reaction processes is usually not considered due to electron self-interaction errors of the standard semilocal functionals that cannot properly describe EPs.[36] Second, the polaronic effects and polaron interactions with reactants significantly complicate excited-state modeling. Third, EP dynamics and EP interactions with free carriers leading to nonradiative charge losses are simulated rarely, especially in the presence of adsorbates, since such simulations require advanced simulation methodologies. In order to address these issues, we have carried out *ab initio* molecular dynamics (AIMD) and *ab initio* NA molecular dynamics (NA-MD)[37,38] simulations combined with real-time time-dependent density functional theory (TD-DFT) in the Kohn−Sham formalism[39−41] to study polaron localization and hopping in the O_V/TiO_2 system, adsorption of the CO molecule and its interaction with EPs, and nonradiative recombination of EPs with holes. Our results show that the polaron distribution has a significant influence in the initial adsorption of the CO molecule, which prefers to occupy a specific site next to the surface EP associated with a Ti atom in the +3 oxidation state. The strong CO−polaron interaction enhances the CO adsorption and stabilizes the polaron at the surface, allowing it to participate in chemical reactions. In addition, the CO molecule suppresses polaron hopping. The partial localization of the surface EP on the CO molecule decouples it from the free hole and prolongs the lifetimes of both the EP and the free hole. The study establishes the mechanisms underlying efficient photochemical activity of reduced TiO_2 in the presence of adsorbates and indicate that EPs have significant influence in the initial adsorption step. Inversely, the adsorbate has a strong influence on the polaron localization, polaron−phonon coupling, and lifetime. Our results show that adsorbate−polaron interactions can be tuned to design high-performance devices based on TMOs.

2. COMPUTATIONAL METHODS

The electronic structure calculations and AIMD were carried out using the Vienna *ab initio* simulation package within the framework of spin-polarized DFT.[42] The generalized gradient approximation of Perdew−Burke−Ernzerhof[43] (PBE) was used, in combination with the on-site Coulomb correction[44] applied to titanium (Ti) 3d electrons (U = 4.2 eV) to describe the small polarons in TiO_2, referring to the previous report.[45] The projector augmented wave (PAW) potentials[46] were employed with the semicore electrons of O $2s^2 2p^4$ and Ti $3s^2 3p^6 4s^2 3d^2$. The energy cutoff was set to 500 eV. The Gaussian smearing value is set to 0.05 eV. Density of states (DOS) calculations were also performed using the hybrid HSE06 functional.[47] The energy convergence criterion of the electronic self-consistent field was 10^{-5} eV, and the structures were relaxed until the

https://doi.org/10.1021/jacsau.1c00508
JACS Au 2022, 2, 234−245

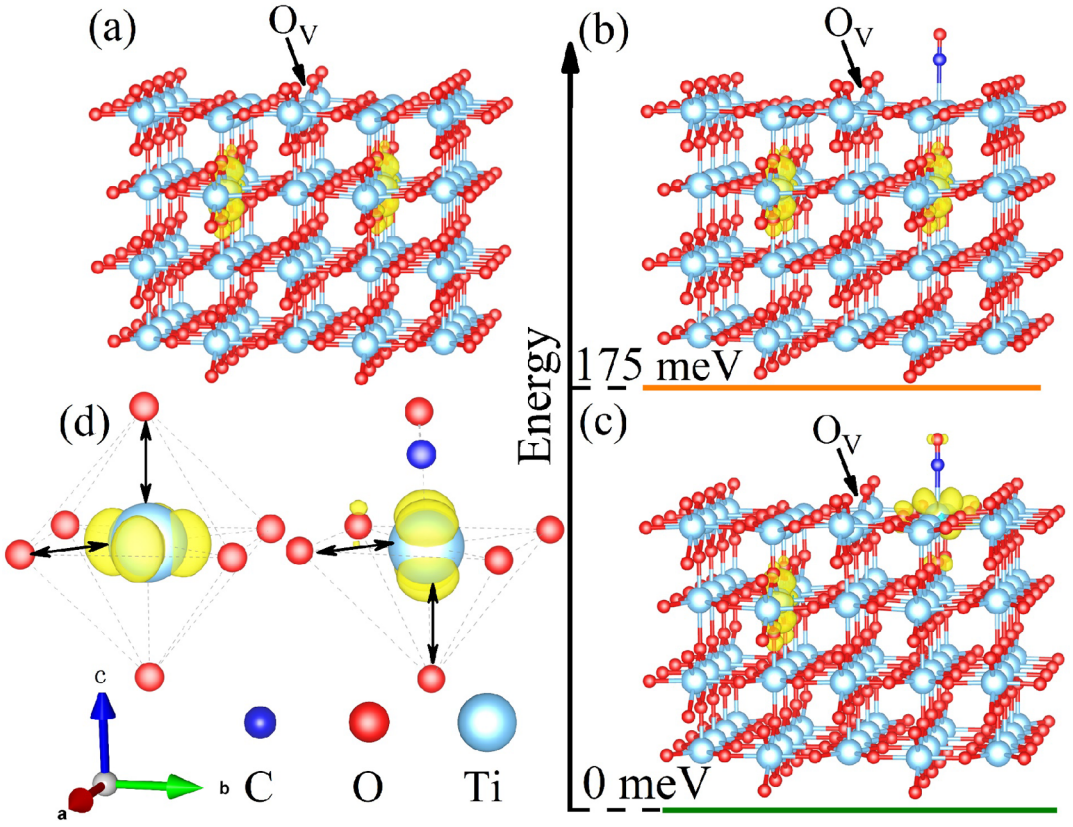

Figure 1. (a) The optimized structure of the two EP model induced by an oxygen vacancy (O_V/TiO_2). (b) Optimized structure of the two EP system with a CO molecule adsorbed on the TiO_2(110) surface with the oxygen vacancy, with both polarons remaining in subsurface. (c) Same as part (b) but with one of the polarons occupying the surface site next to the CO molecule. The relative energies shown in parts (b) and (c) indicate that a polaron prefers to hop to the surface site. (d) Schematic of EP formation by elongating Ti−O bonds in the TiO_6 octahedra in the bulk and the TiO_5 pentahedron on the surface. The EP charge densities are shown in yellow. The structures are visualized using the VESTA software.[85]

ionic forces were <0.02 eV·Å^{-1}. Shown in Figure 1, the O_V/TiO_2 and CO/TiO_2 models contain four O−Ti−O layer (4 × 2) supercell slabs with 191 and 193 atoms, respectively. The bottom layer was fixed to maintain the bulk properties. This model is often used to represent the rutile TiO_2 (110) surface to model experimental phenomena.[19,29,48−52] A 15 Å vacuum layer was added in the direction perpendicular to the surface to minimize interactions between periodic images. The van der Waals interactions were included using the Grimme DFT-D3 method.[53,54] The local magnetic moment was used to identify the EP sites in the MD simulations.

After relaxing the geometries at 0 K, the systems were brought up to 300 and 700 K by repeated velocity rescaling using the spin-polarized PBE+U DFT functional at the Γ-point. Then 10 ps microcanonical AIMD trajectories were generated with a 1 fs time step. These trajectories were used for further analysis and as initial conditions for the NA-MD simulations. To guarantee good statistical convergence, 1000 initial conditions were randomly sampled from the 10 ps trajectories, and 1000 stochastic realizations of the surface hopping algorithm were generated for each initial geometry. The NA-MD simulations were performed using the python extension for ab initio dynamics (PYXAID) code.[37,38] The decoherence-induced surface hopping (DISH) algorithm[55] and the classical path approximation[56] were employed, as implemented within the time-dependent Kohn−Sham DFT.[39−41] Phase tracking was applied to correct the arbitrary phase in the adiabatic wave functions.[57] The NA coupling (NAC) was computed with the PAW potentials.[58,59] Although it is preferable to treat atomic motions quantum mechanically, it is not possible for practical reasons. The systems contain hundreds of atomic degrees of freedom, and if, for example, one uses 10 basis states per degree of freedom, the required quantum mechanical basis set becomes astronomical, on the order of 10.[100] For this reason, semiclassical treatment remains the only choice. It also is not possible to focus quantum mechanically on the few most important degrees of freedom, because such degrees of freedom are hard to identify and since other motions can have a profound collective effect. The semiclassical correction is introduced via the decoherence time, which is determined by fluctuations of the energy gap. Typically larger gaps produce larger fluctuations, leading to faster decoherence,[37] which slows down the transition time, according to the quantum Zeno effect.[60] Larger gaps correspond to slower transitions in our simulations, following the energy gap law.[61] This approach was applied successfully to investigate excited-state dynamics in a broad range of systems, including metal oxides,[62−67] layered materials,[68−73] perovskites,[13,74−79] etc.[80−83]

Static calculations for optimized geometries corresponding to 0 K show positions and energies of EPs. Thermal atomic fluctuations cause geometric distortions, which change both energies and locations of EPs. Such fluctuations are not known from the 0 K calculations and are most naturally studied by AIMD. Study of nonradiative recombination of EPs requires NA-MD capabilities that extend beyond most standard electronic structure codes. Even codes that contain NA-MD capabilities may be hard to use in the present case due to system size or methods implemented, for example, the most common Ehrenfest (mean-field) method cannot describe electron-vibrational relaxation to thermodynamics equilibrium.[84]

3. RESULTS AND DISCUSSION

We consider two systems, see Figure 1. The EPs are formed by removing a surface bridge oxygen in rutile TiO_2(110), giving the O_V/TiO_2 model. The CO/TiO_2 system is created from the O_V/TiO_2 model by adding the CO molecule to the nearest-neighbor NNN-Ti_{5c} site, as established in ref 32. In order to

https://doi.org/10.1021/jacsau.1c00508
JACS Au 2022, 2, 234−245

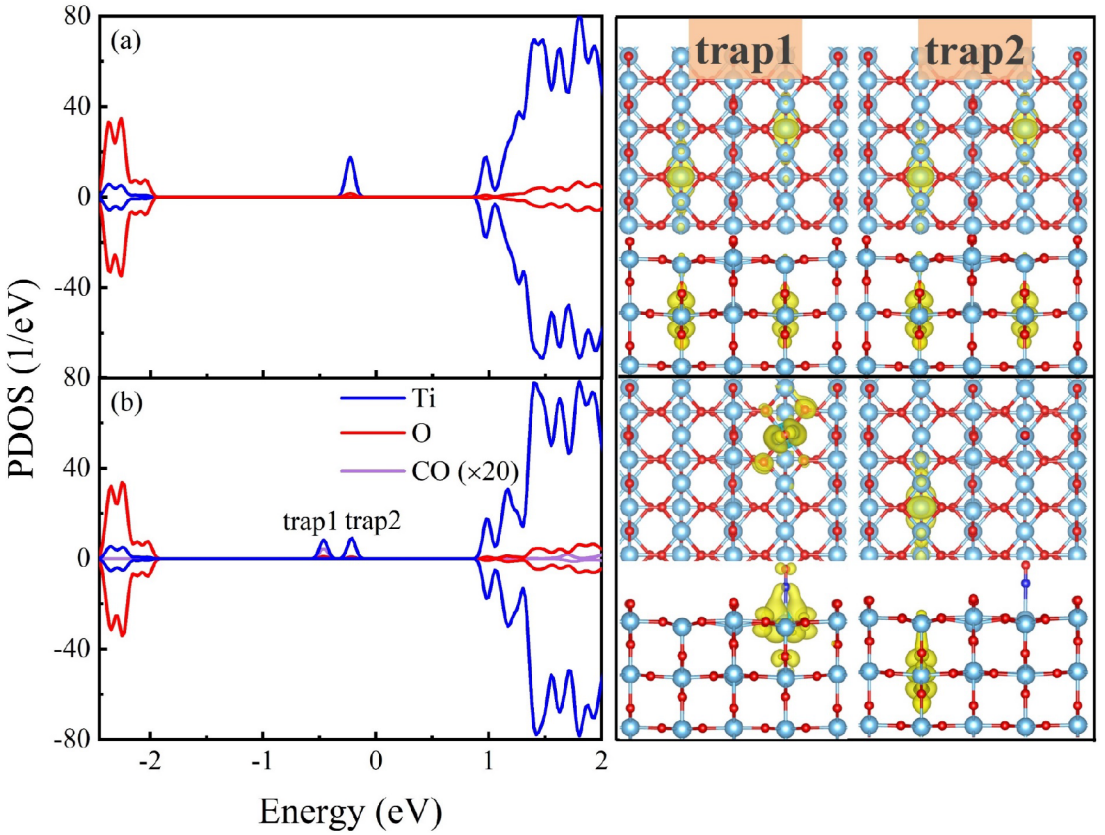

Figure 2. PDOSs of (a) O_V/TiO_2 and (b) CO/TiO_2, calculated with the HSE06 functional using the optimized geometries. The PDOSs are separated into contributions from O, Ti, and CO. The Fermi level is set to zero. The midgap states induced by the oxygen vacancy are degenerate in the O_V system, while they split in the CO system. The charge densities of the midgap states are shown on the right.

investigate CO adsorption influences the EP dynamics, we perform AIMD and NA-MD simulations. Section 3.1 focuses on the geometric and electronic structures of the two EP systems. Section 3.2 discusses adiabatic dynamics of the EPs with and without the CO molecule and CO adsorption stability on the reduced TiO_2 with the EPs on the surface and subsurface. Section 3.3 details elastic and inelastic electron−vibrational interactions in the O_V/TiO_2 and CO/TiO_2 systems. Section 3.4 compares electron−hole recombination processes in O_V/TiO_2 and CO/TiO_2.

3.1. Geometric and Electronic Structure at 0 K

TiO_6 octahedra are basic building blocks in the inner rutile. Each O atom is 3-coordinated, and each Ti atom is 6-coordinated. The most stable EP structure of reduced rutile TiO_2(110) with a surface two-coordinate oxygen vacancy is obtained by stretching six Ti−O bonds by 0.1 Å (Figure 1d) and then optimizing the geometry, localizing the excess electrons on the central Ti atoms of the TiO_6 octahedra, as shown in Figure 1a. The two excess electrons are supported by 3d orbitals of the two subsurface Ti atoms (Ti_{23} and Ti_{47}, see site labels in Figure S1) just below the surface Ti_{5c} atoms. About 80% of the excess charge is confined at the center Ti atom of the TiO_6 octahedron, while the remaining 20% of the charge is mainly spread around the surrounding oxygen atoms. The localized electron distorts the lattice and gives rise to an elongation of the nearest Ti−O bonds, with the equatorial and apical bonds extended by approximately 0.090 and 0.036 Å, respectively. This geometrical expansion weakens the Jahn−Teller distortion and localizes the excess electrons at the center Ti atoms. Our polaron configuration agrees well with the lowest-energy polaron model in the previous reports.[16,19,27,86] Inspired by the experimental reports that CO molecules induce polaron transfer from subsurface to a surface Ti_{5c} underneath CO[10,27] and that CO preferentially adsorbs on the NNN-Ti_{5c} site next to O_V rather than the O_V site itself,[27,32] we build two CO/TiO_2 model configurations. Either both polarons are localized at the subsurface, representing the situation in which CO just got adsorbed on reduced rutile TiO_2(110) without changing the two EPs locations (Figure 1b) or one polaron is at the subsurface, while the other migrates to the surface, which is achieved by elongating the five Ti−O bonds at the polaron site by 0.1 Å and optimizing the geometry (Figure 1c). In the latter case, 84% of the surface EP density is localized at the surface Ti_{5c} (Ti_{44}) atom. This is greater than the 80% localization of the subsurface polaron on the central Ti atom. Transfer of an EP from the subsurface to the surface enhances the CO adsorption and lowers the system's energy by 175 meV. The calculated CO adsorption energies are −0.57 eV and −0.79 eV, shown in Figure 1b,c, respectively, indicating the surface EP enhances CO adsorption.[10,33] The more stable CO adsorption configuration (Figure 1c) is considered below in more detail.

Figure 2 displays the spin-polarized projected densities of states (PDOSs) and EP charge densities for O_V/TiO_2 and CO/TiO_2. The PDOSs are split into contributions from Ti and O atoms, and the CO molecule. The conduction band minimum (CBM) and valence band maximum (VBM) are primarily composed of the Ti and O atomic orbitals, respectively. Due to the self-interaction error of the PBE

https://doi.org/10.1021/jacsau.1c00508
JACS Au 2022, 2, 234−245

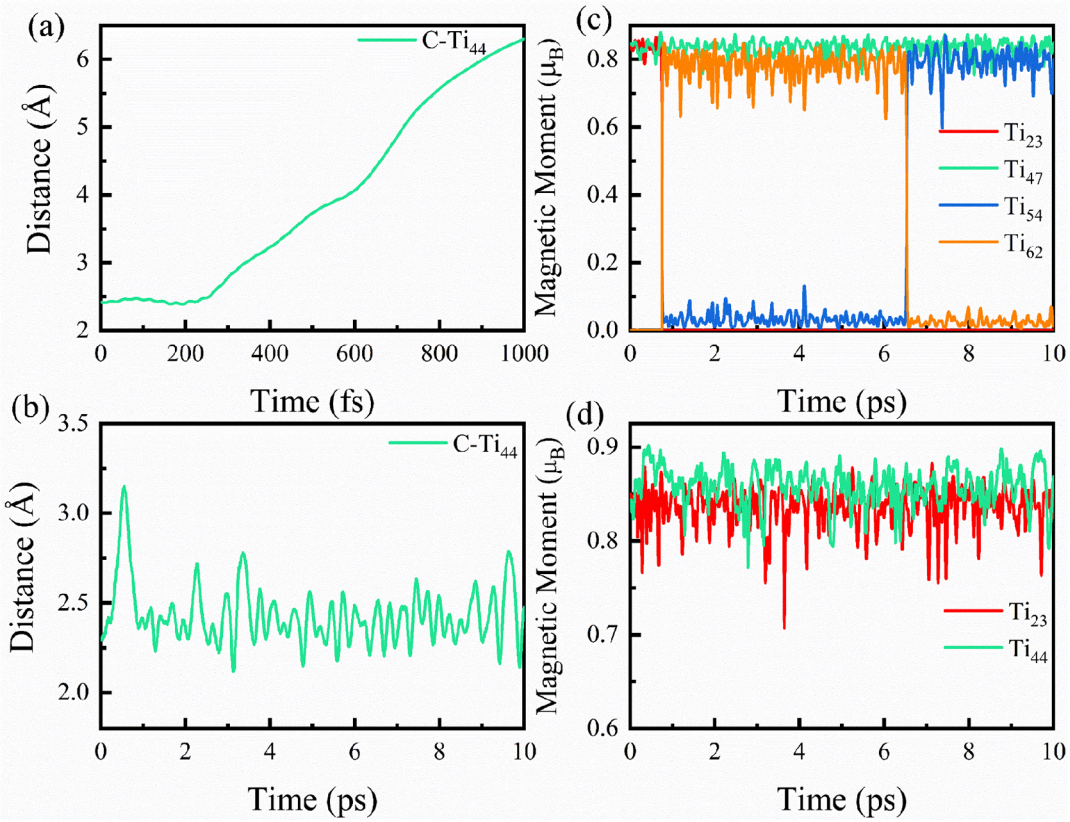

Figure 3. Distances between the C atom of the CO molecule and the Ti atom (Ti_{44}) next to it when (a) both polarons are sublayer and (b) one of the polarons is localized next to the CO molecule (Figure 1b,c), respectively. The CO molecule desorbs after 200 fs (a), unless the EP is localized next to it (b). Electron polaron hopping is reflected by changes of the local magnetic moments on Ti atoms for (c) O_V/TiO_2 and (d) CO/TiO_2. The data correspond to 300 K. The optimized geometry for CO adsorption on the defective TiO_2(110) with both polarons staying in the sublayer is shown in Figure S6. The surface EP enhances adsorption of the CO molecule, preventing its desorption. Inversely, the CO molecule stabilizes the surface polaron, preventing hopping into subsurface. Both phenomena are beneficial for catalytic processes, such as CO reduction.

functional, the bandgap cannot be accurately described. The HSE06 functional[47] is used to calculate the electronic structure based on the geometry optimized with PBE+U. The calculated bandgap of 2.57 eV agrees with the previous theoretical report,[87] which employed the same code, simulation cell, and calculation parameters. Notably, other works report different bandgaps.[88,89] The differences may arise from several factors, including oxygen vacancies, simulation cell size, basis set, core pseudopotential, and implementation with a particular simulation package. For instance, Esch et al. obtained a 3.35 eV bandgap with a pristine (1×1) rutile TiO_2 (110) unit cell using the HSE06 functional with the triple-ζ plus polarization basis set, implemented in the CRYSTAL14 code.[88] Wen et al. used the (4×2) rutile TiO_2(110) supercell with an oxygen vacancy and obtained a 3.62 eV bandgap with a hybrid Gaussian/plane-wave basis and the CP2K/Quickstep package. The core electrons were described with norm-conserving Goedecker−Teter−Hutter pseudopotentials, and the wave functions of the valence electrons were expanded in Gaussian functions using the molecularly optimized double-ζ polarized basis sets.[89] In order to account for the systematic error, we scale the bandgap to the experimental gap of 3.0 eV using the "scissor operator". For the O_V/TiO_2 case (Figure 2a), two quasi-degenerate EP states obtained by setting the electron smearing value to 0.05 eV are found 1.13 eV below the CBM, which is consistent with ∼1.0 eV reported in the previous publications.[86,87] The smearing value 0.05 eV is significantly smaller than the band gap of the O_V/TiO_2 and CO/TiO_2 systems and is suitable for the present simulation.[90] Additional tests are reported in Figure S2. The lowest-energy state of the O_V system is triplet, with excess electrons forming EPs in the same spin channel, in agreement with the previous reports.[16,19] Analysis of the PDOS, magnetic moment, and charge densities allows a convenient identification of the two EPs. The EP states can trap holes, and recombination of EPs with holes eliminates both types of charge carriers. The charge densities of the quasi-degenerate trap1 and trap2 states, shown in the right panel of Figure 2a, are very similar and are localized in the second layer, reflecting symmetrical EP distribution with respect to the vacancy site.

CO alters the symmetrical distribution of the EPs and splits the degenerate energy levels (Figure 2b). The lower trap1 EP state is ∼0.25 eV below the trap2 EP. Strong orbital hybridization between the trap1 EP and the CO molecule reflects strong interaction between them,[10] which enhances CO adsorption. To reveal the influence of CO on the EP orbital characteristics, the localized DOSs of the special Ti^{3+} EP are shown in Figure S3. The EP distributed in the sublayer (Ti_{47}) shows the d_{z^2} symmetry, together with a smaller $d_{z^2-y^2}$ contribution, in agreement with the previous report.[91] On the contrary, the surface EP coupled with the CO molecule and exhibits the d_{yz} symmetry with a smaller d_{xz} orbital contribution, indicating that CO alters the EP orbital characteristics. The CO molecule switches the d_{z^2} orbital,

https://doi.org/10.1021/jacsau.1c00508
JACS Au 2022, 2, 234−245

Table 1. Canonically Averaged Energy Gap, Absolute NAC, Pure-Dephasing Time, Energy Gap Fluctuation, and Time of Nonradiative Electron-Hole Recombination between the VBM and Trap1 in O_V/TiO_2 and CO/TiO_2

	energy gap (eV)	NAC (meV)	dephasing (fs)	gap fluctuation ($10^{-3}eV^2$)	recombination (ns)
O_V/TiO_2	1.70	0.51	4.94 ± 0.025	15.8	3.01 ± 0.31
CO/TiO_2	1.60	0.48	4.34 ± 0.001	20.0	3.48 ± 0.20

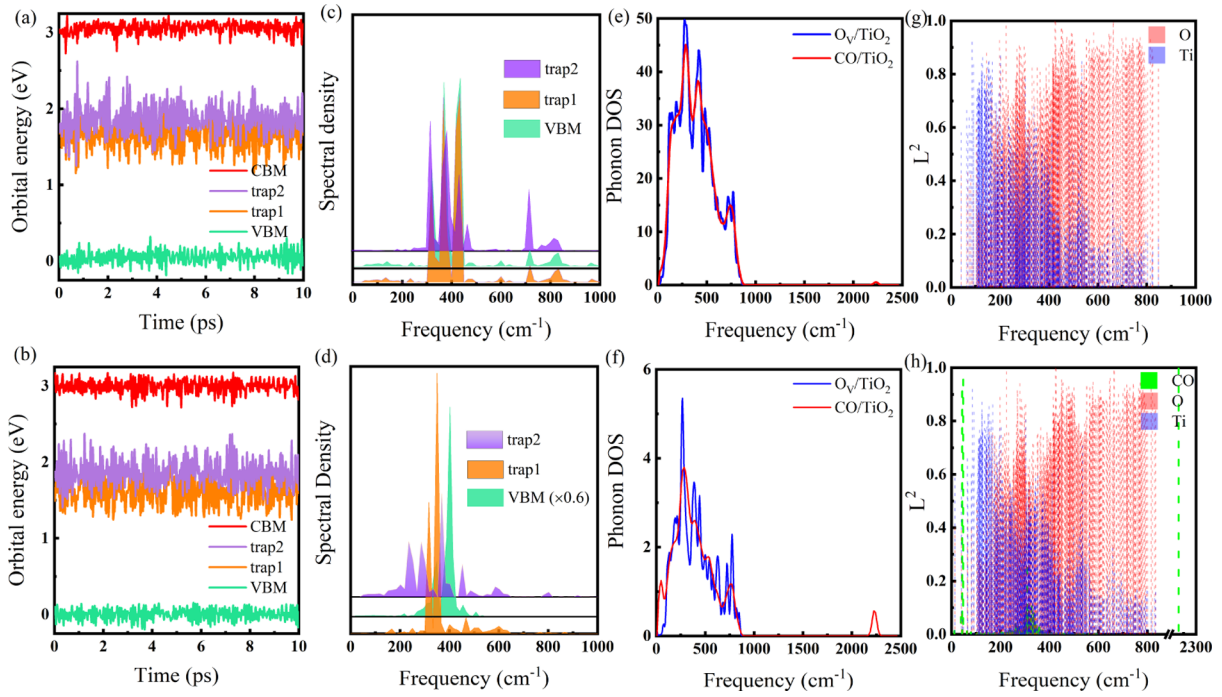

Figure 4. (a, b) Evolution of orbital energies of the key electronic states in the O_V/TiO_2 and CO/TiO_2 systems. (c, d) Corresponding spectral densities obtained by Fourier transforms of autocorrelation functions of fluctuations of the VBM, trap1, and trap2 energies. Phonon DOS for (e) the whole system and (f) local polaron states. Spatial localization of modes in (g) O_V/TiO_2 and (h) CO/TiO_2. The phonon modes are projected into O, Ti, and CO contributions. CO softens the phonons and shifts them to lower energies.

which is dominant in the subsurface EP, to the more energetic d_{yz} orbital in the surface EP. The charge densities of the EPs obtained using the PBE+U functional are shown in Figure S4. They are nearly the same as those obtained with the HSE06 functional, indicating that PBE+U provides a good description of the polaron properties. To save the computational resources, the sequent AIMD and NA-MD simulations are performed with the PBE+U functional.

3.2. Interplay between the Adsorbed CO Molecule and the Electron Polarons

To elucidate the influence of the EPs on CO adsorption, we investigate the CO adsorption configurations with the EPs polarons in either the subsurface or the surface (Figure 1b,c). Figure 3a,b reports the Ti−C bond lengths for the two EP polarons models, in order to characterize the stability of adsorbed CO at 300 K. Figure 3a shows that the adsorption of CO is very weak if both polarons are in the subsurface. The CO desorbs within ∼200 fs after the heating. When an EP stays at the surface (Figure 1c), the strong CO−polaron interaction stabilizes the CO molecule, which remains adsorbed after 10 ps (Figure 3b). The stability of the adsorbed CO benefits the CO reduction process that can lead to sustainable production of chemical and fuels.

In order to reveal the influence of EP−CO interactions on EP localization, we monitor charge localization along the 10 ps AIMD trajectories at 300 K by computing the occupation matrix of each Ti spin orbital.[16] Figure 3c,d shows the local magnetic moments on Ti ions along the AIMD trajectories in the O_V/TiO_2 and CO/TiO_2 systems. Upon formation of an EP in TiO_2, a Ti^{4+} ion is reduced to a Ti^{3+} ion with the local magnetic moment formally increased from 0 to 1 μB. The calculated magnetic moments are very close to this value, as reported by Kowalski et al.[16] For the O_V/TiO_2 case, as demonstrated in Figure 3c, the trap1 EP transfers from Ti_{23} in the second layer to Ti_{62} in the third layer in about 0.8 ps. Then, the EP transfers to the adjacent Ti_{54} in the third layer in <7 ps during the short 10 ps simulations. At the same time, the trap2 EP remains in the second layer. In order to validate the model and calculated parameters, we conduct an AIMD simulation at 700 K (Figure S5). The results show that both the EPs hop to different sites frequently, and there are many instances when the EPs hop to surface sites, agreeing well with the previous reports.[16,91] Thus, the EPs can hop to surface active sites at elevated temperatures without assistance of the CO molecule and participate in a catalytic process. However, diffusion of the EPs to the surface is less likely at low temperatures. This process can be assisted by the CO molecule, promoting the subsequent chemical processes, as elucidated by STM measurements.[10] The EP polaron in the surface layer is very stable when interacting with the CO molecule, and the second-layer EP is also stable at 300 K (Figure 3d). The EPs hopping events have not occurred in the CO/TiO_2 system at 300 K when the CO−polaron complex present.

https://doi.org/10.1021/jacsau.1c00508
JACS Au 2022, 2, 234−245

Thus, the EPs associated with O_V in the O_V/TiO_2 system exhibit polaron−polaron repulsion in the subsurface, and an elevated temperature promotes EPs hopping. In contrast, the strong CO−polaron coupling in the CO/TiO_2 system reduces the polaron−polaron interaction, in particular, since the polarons become spatially separated. By suppressing polaron hopping and keeping the EP on the surface, the CO molecule facilitates transfer of electrons from TiO_2 bulk to surface, where they can participate in catalysis at low temperatures. The calculations show that the energy of the lowest unoccupied molecular orbital of CO is higher than the energies of the EP states. Therefore, the EPs cannot be captured by the CO molecule. The recent X-ray photoelectron spectroscopy (XPS) data show that oxygen defects in rutile act as charge traps that drive chemical reactions rather than lead to charge recombination, improving the photocatalytic performance by almost 100% compared with the stoichiometric surface.[92] Our results demonstrate that CO adsorption at the NNN-Ti_{5c} site, observed in the STM experiments,[32] stabilizes the EP beneath it, enhancing catalytic activity.

3.3. Electron−Vibrational Interactions

Electron−vibrational interactions cause inelastic and elastic electron−phonon scattering. Both types of scattering affect recombination dynamics. The NAC reflects inelastic electron−phonon scattering, which is computed between the initial (EP) and final (ground) states. The average absolute NAC is reported in Table 1. Elastic scattering destroys coherence formed between the initial and final states. The coupling of the EP and other electronic states to vibrational motions can be characterized by phonon driven fluctuations of the state energies (Figure 4a,b), and Fourier transforms of the energy autocorrelation functions (ACF) (Figure 4c,d) are known as the influence spectra or spectral densities.[37] The amplitude of the energy fluctuations reflects the strength of the electron−vibrational interaction, while the frequencies of the oscillation identify the phonon modes involved.

Figure 4a,b shows evolutions of the orbital energies for the key states in the O_V/TiO_2 and CO/TiO_2 system. The energy levels of the trap1 and trap2 states of the EPs are no longer degenerate in the O_V/TiO_2 system at 300 K due to breaking of the lattice symmetry by thermal motions and EP hopping (Figure 4a), in contrast to the 0K calculation (Figure 2a). Interestingly, a large number of lower frequency signals are seen in the CO/TiO_2 system (Figure 4d) than the O_2/TiO_2 system (Figure 4c), even though CO itself is light and vibrates fast. The lower frequencies arise from the motion of the CO molecule relative to the TiO_2 surface and coupling of CO to the EPs. Focusing on the most important transition between trap1 and VBM, we report Fourier transforms of the trap1-VBM energy gaps in Figure S7, which shows similar results. Lower frequency modes become more prominent after CO adsorption. The higher peak intensities in the CO/TiO_2 system, rationalizing the faster elastic scattering, are characterized by the pure-dephasing time,[37] 4.34 fs vs 4.94 fs (Table 1). At the same time, involvement of lower frequency modes leads to a smaller NAC value, 0.48 meV vs 0.51 meV, since the NAC is proportional to vibrational velocity,[37] which is smaller for lower frequency vibrations at a fixed temperature. The NAC also depends on the overlap between the initial and final states. The interaction between CO and the EPs results in EP delocalization onto the CO molecule and its decoupling from the TiO_2 VBM and CBM, further decreasing the NAC.

To further explore the influence of CO on the vibrational properties, we report the overall phonon DOS (Figure 4e) and its decomposition into atomic contributions (Figure 4g). The vibrational frequencies seen in Figure 4e are below 1000 cm^{-1}, corresponding the Ti−O vibrations.[93] Interestingly, the intensities of the peaks are slightly suppressed after introduction of the CO molecule. To characterize the phonon modes present in the EPs, we present analogous data for the two TiO_6 octahedra supporting the EPs in O_V/TiO_2 and the TiO_6 octahedron and the TiO_5 pentahedron coupled to the CO molecule, supporting the EPs in CO/TiO_2 (Figure 4f,h). The phonon DOS associated with the EPs show finer structure, and the CO/TiO_2 spectrum exhibits new frequencies associated with the CO stretching motion at 2200 cm^{-1} and vibration of CO relative to TiO_2 at the very low frequency below the TiO_2 signals (Figure 4f). Analysis of the spatial localization of the modes[94] (Figure 4g,h) confirms the above conclusions. Ti−O vibrations dominate the spectra, and higher frequency TiO_2 modes exhibit stronger contributions from the lighter O atoms. The CO stretching frequency of 2220 cm^{-1} agrees with the experimental value of ∼2190 cm^{-1}.[27] Contributions from the CO molecules are seen around 300 cm^{-1} (Figure 4h). They correspond to Ti−CO stretching and bending. The frequency at ∼40 cm^{-1} is assigned to quasi-translation motion of CO relative to the TiO_2 surface.[95]

The TiO_2 lattice is quite rigid, and the CO molecule is light and moves fast. Therefore, the system equilibrates fast, and all relevant motions occur multiple times within the 10 ps simulation. We do not consider surface diffusion of the CO molecule. The CO molecule adsorbed in the system with both EPs occupying subsurface sites desorbs within 200 fs (Figure 3a). Hopping of EPs between different sublayer atoms in the Ov/TiO_2 system requires several picoseconds and cannot be properly sampled during the 10 ps simulation. However, EP hopping away from the surface layer is not particularly important for catalysis, which depends on EP presence on the surface. Therefore, we do not study the subsurface hopping in detail. Nonradiative recombination of EPs with holes occurs by coupling to vibrations with frequencies between 100 and 1000 cm^{-1} (Figure 4c,d). Oscillation with a 1 ps period corresponds to 33.4 cm^{-1}, and oscillation with 10 ps period corresponds to 3.34 cm^{-1}. Therefore, all relevant frequencies are represented well in the 10 ps trajectories. The evolution of the total energy of the CO/TiO_2 system during the 10 ps MD simulations is stable (Figure S8), indicating that the system is in equilibrium. Performing AIMD and NA-MD for longer times for systems of this size is computationally expensive. Our previous simulations using trajectories of similar length showed good results for a broad range of materials, including pristine and doped TiO_2 and TiO_2 sensitized with other semiconductors.[62,71,96,97]

Figure S9 presents the pure-dephasing functions for the energy gap between the VBM and trap1 states. Pure-dephasing occurs by elastic electron−phonon scattering and characterizes the duration of coherence between the electronic states. The pure-dephasing functions are computed using the second-order cumulant approximation of the optical response theory:[98]

$$D_{ij}(t) = \exp\left(-\frac{1}{\hbar^2}\int_0^t dt' \int_0^{t'} dt'' C_{ij}(t'')\right) \quad (1)$$

where $C_{ij}(t'')$ is the unnormalized ACF of the phonon-induced fluctuation of the energy gap, $\delta E_{ij}(t')$, between states i and j:

https://doi.org/10.1021/jacsau.1c00508
JACS Au 2022, 2, 234−245

$$C_{ij}(t) = \langle \delta E_{ij}(t')\delta E_{ij}(t - t')\rangle_{t'} \quad (2)$$

Fitting each of the curves to a Gaussian, $\exp(-0.5(t/\tau)^2)$, gives the pure-dephasing times reported in Table 1. The results point out that coherence loss is faster in CO/TiO_2 than O_V/TiO_2, 4.34 fs vs 4.94 fs, because the energy gap fluctuates with a larger amplitude. This is reflected in the high peaks in the spectral density (Figure 4c,d) and the larger initial ACF value (Table 1). The initial value of the unnormalized ACF is equal to the square of phonon-induced energy gap fluctuation.[37] According to the quantum Zeno effect,[60] fast decoherence slows down quantum dynamics. The smaller NAC and shorter pure-dephasing time (Table 1) suggest that CO/TiO_2 system should exhibit slower nonradiative electron−hole recombination.

3.4. Nonradiative Charge Carrier Recombination

To reveal the impact of the CO molecule on the EP and free carrier lifetimes, the electron−hole recombination dynamics between the VBM and the lowest-energy EP state, trap1, are investigated, Figure 5. The initial states for the NA-MD

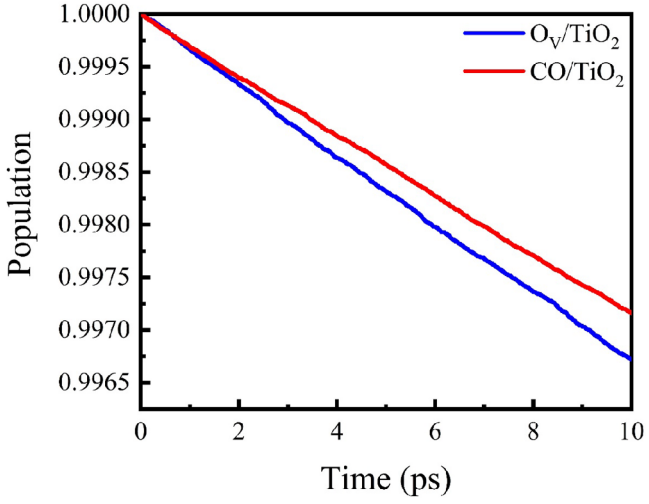

Figure 5. Electron−hole recombination dynamics in the O_V/TiO_2 and CO/TiO_2 systems. Shown are populations of the excited states that decay nonradiatively to the ground states.

simulation of the nonradiative electron−hole recombination in both O_V/TiO_2 and CO/TiO_2 systems are electron−hole pairs, with the electron in the lowest-energy EP state, trap1, and the hole in the VBM. The corresponding charge densities are shown in Figures 2, S2, and S4. Trap1 is localized on the sublayer Ti_{47} atom in O_V/TiO_2 (Figure S2) and on the Ti_{44} atom next to the adsorbed CO molecule in CO/TiO_2 (Figure S4). Fitting the data in Figure 5 to the short-time linear approximation to the exponential function, $P(t) = \exp(-t/\tau) \approx 1 - t/\tau$, gives the nonradiative electron−hole recombination times (Table 1). The calculated carrier lifetime is slightly longer in CO/TiO_2 than O_V/TiO_2, 3.48 ns vs 3.01 ns, and agrees well with the previous experimental and theoretical reports.[99,100] In order to test the robustness of the obtained results, we divided the 1000 initial conditions into 5 equal parts containing 200 configurations each, repeated the NA-MD simulations separately for each set of 200 configurations, and calculated the standard deviations. The data shown in Figure S10 support the original results (Figure 5). According to Fermi's golden rule, the recombination time is proportional to the inverse of the NAC squared. Also, it increases with decreasing coherence time. These two factors rationalize the slight extension of the lifetime upon the adsorption of CO. The EP in the CO/TiO_2 system decouples from the VBM, because it localizes to some extent on CO and, thus, overlaps less with the VBM that is supported mainly by the O atoms of TiO_2 (Figure 2). The reduced electron−hole overlap decreases the NAC and shortens the coherence time by making fluctuations of the VBM and trap1 energies less correlated. In addition, CO decreases the electron−phonon coupling by suppressing EP hopping (Figure 3) and softening the phonon modes (Figure 4). The surface EPs delocalize on the CO molecule only partially. Therefore, other chemical species are required in order to complete CO reduction. Alternatively, the adsorbed CO may promote other types of photochemistries by making the excess electrons available for the chemically active species.

Thus, we demonstrate that adsorbates, such as CO, can induce EP transfer from the subsurface to the surface. The dynamics of the CO-polaron complex are investigated by AIMD, and the results show that the CO molecule suppresses polaron hopping. The nonradiative electron−hole recombination times are also evaluated, indicating that the CO molecule slightly prolongs the carrier lifetime, which decreases carrier losses. Overall, more charge carriers can become available at the surface to interact with reactants and drive photochemical reactions.

Our theoretical results rationalize the experimentally observed high CO photo-oxidation activity on rutile $TiO_2(110)$.[35] First, in the photo-oxidation of CO Xu et al.[35] exposed rutile $TiO_2(110)$ to CO first, and then they exposed the surface to both molecular oxygen gas and UV photons. The CO adsorption was very stable, and our studies demonstrated that only CO interacting with the EP at the surface Ti_{5c} site forms a stable species, avoiding desorption and subsequently taking part in the oxidation process. Second, the recent XPS experiments show that defects in rutile acting as charge traps improve the photocatalytic performance by almost 100%,[92] rather than acting as charge recombination centers. Our simulations confirm this observation by showing that traps can effectively transfer charges to reactant species. Finally, the calculated CO vibration frequency in the CO/TiO_2 system is close to the experimental IR peak.[27,35] Our calculations demonstrate the oxidation state of the surface NNN-Ti_{5c} site stemming from the O_V defect is +3, creating the Ti^{3+} EP. The active site favors charge transfer to reactants and promotes subsequent chemical processes.

4. CONCLUSIONS

Using a combination of DFT, AIMD, real-time TD-DFT, and NA-MD, we have investigated EP properties and nonradiative EP-hole recombination in the O_V/TiO_2 and CO/TiO_2 systems, with particular emphasis on the influence of CO adsorption on polaron dynamics at the TiO_2 surface. The static DFT calculations demonstrate that an oxygen vacancy at the rutile $TiO_2(110)$ surface gives rise to two EPs in the subsurface and leads to CO adsorption on a surface NNN-Ti_{5c} site. In the absence of CO, the EPs hop rapidly between different lattice sites; however, they remain below the surface and, therefore, cannot participate in catalytic surface reactions. The AIMD simulations clarify the nature of the most favorable CO adsorption site on the defective rutile $TiO_2(110)$ surface, providing an interpretation of the STM measurements.[32] The CO molecule prefers to adsorb at the NNN-Ti_{5c} atom, leading

https://doi.org/10.1021/jacsau.1c00508
JACS Au 2022, 2, 234−245

to formation of a surface EP Ti^{3+}. Without the surface EP, the CO molecule easily desorbs from the rutile TiO_2(110) surface even in the presence of subsurface EPs. However, the surface Ti_{5c} polaron enhances the adsorption strength and prevents CO desorption. In return, the CO molecule shifts the EP from the d_{z^2} orbital to the lower energy d_{yz} orbital and alters EP stability, suppressing EP hopping to other lattice sites. The strong CO−polaron interactions change the chemical properties of the TiO_2 surface, having a significant impact on the its catalytic reactivity. Our results show that, apart from the polaron engineering by an STM tip, polarons can be controlled by CO molecules and other adsorbed species without sacrificing the charge carriers, which remain chemically active.

The NA-MD simulation establishes that the adsorbed CO does not shorten the EP lifetime, even though one has such expectation *a priori*, due to the fact that CO stretching vibration is fast and can promote rapid nonradiative relaxation. NA-MD demonstrates the opposite effect. Localization of the EP on the surface next to the adsorbed CO molecule slightly increases the charge carrier lifetime. The increase in the carrier lifetimes is associated with the partial localization of the EP on the CO molecule and, hence, its separation from the free hole that resides in TiO_2. The EP-hole separation decreases their overlap and correlation, thereby reducing the NA coupling and shortening the coherence time. The latter two factors favor longer carrier lifetimes, increasing the chance that the carriers participate in a chemical reaction.

Our simulations demonstrate the importance of the initial stages of photocatalytic reactions on reduced TMO surfaces associated with molecular adsorption. The coupling between the CO molecule and the EPs is favorable for the properties of both species. The CO adsorption is enhanced, the charge carrier is attracted to the surface, and the carrier lifetime increases. The simulations establish the mechanisms responsible for the influence of CO adsorption on activity of reduced TiO_2(110), advance our understanding of adsorbate−polaron interactions in photocatalytic systems, and indicate that knowledge of the adsorbate−polaron interactions is important for design of better TMO photocatalysts.

■ ASSOCIATED CONTENT

Supporting Information

The Supporting Information is available free of charge at https://pubs.acs.org/doi/10.1021/jacsau.1c00508.

Numerical labels of Ti atoms, additional PBE+U calculations with different electron smearing, d-orbital characters of surface and subsurface polarons, EP charge densities obtained with PBE+U, locations of the EP during MD simulations at 300 and 700 K, Fourier transforms of VBM-trap1 energy gaps, total energy evolution during AIMD, pure-dephasing functions for charge recombination in the O_V/TiO_2 and CO/TiO_2 systems, NA-MD calculations with subsets of initial conditions, and structural parameters of the optimized O_V/TiO_2 and CO/TiO_2 systems (PDF)

■ AUTHOR INFORMATION

Corresponding Author

Run Long − *College of Chemistry, Key Laboratory of Theoretical and Computational Photochemistry of Ministry of Education, Beijing Normal University, Beijing 100875, P.R. China;* orcid.org/0000-0003-3912-8899; Email: runlong@bnu.edu.cn

Authors

Cheng Cheng − *College of Chemistry, Key Laboratory of Theoretical and Computational Photochemistry of Ministry of Education, Beijing Normal University, Beijing 100875, P.R. China*

Yonghao Zhu − *College of Chemistry, Key Laboratory of Theoretical and Computational Photochemistry of Ministry of Education, Beijing Normal University, Beijing 100875, P.R. China*

Wei-Hai Fang − *College of Chemistry, Key Laboratory of Theoretical and Computational Photochemistry of Ministry of Education, Beijing Normal University, Beijing 100875, P.R. China;* orcid.org/0000-0002-1668-465X

Oleg V. Prezhdo − *Department of Chemistry, University of Southern California, Los Angeles, California 90089, United States;* orcid.org/0000-0002-5140-7500

Complete contact information is available at: https://pubs.acs.org/10.1021/jacsau.1c00508

Notes

The authors declare no competing financial interest.

■ ACKNOWLEDGMENTS

This work as supported by the financial support of the National Science Foundation of China, grant nos. 51861135101, 21973006, and 21520102005. R.L. acknowledges the Recruitment Program of Global Youth Experts of China, and the Beijing Normal University Startup. O.V.P. acknowledges support of the US Department of Energy, grant no. DE-SC0014429.

■ REFERENCES

(1) Fujishima, A.; Zhang, X.; Tryk, D. A. TiO_2 Photocatalysis and Related Surface Phenomena. *Surf. Sci. Rep.* **2008**, *63* (12), 515−582.

(2) Song, F.; Bai, L.; Moysiadou, A.; Lee, S.; Hu, C.; Liardet, L.; Hu, X. Transition Metal Oxides as Electrocatalysts for the Oxygen Evolution Reaction in Alkaline Solutions: An Application-Inspired Renaissance. *J. Am. Chem. Soc.* **2018**, *140* (25), 7748−7759.

(3) Chen, L.; Unocic, R. R.; Hoffman, A. S.; Hong, J.; Braga, A. H.; Bao, Z.; Bare, S. R.; Szanyi, J. Unlocking the Catalytic Potential of TiO_2-Supported Pt Single Atoms for the Reverse Water−Gas Shift Reaction by Altering Their Chemical Environment. *JACS Au* **2021**, *1* (7), 977−986.

(4) Lin, F.; Wang, H.; Zhao, Y.; Fu, J.; Mei, D.; Jaegers, N. R.; Gao, F.; Wang, Y. Elucidation of Active Sites in Aldol Condensation of Acetone over Single-Facet Dominant Anatase TiO_2 (101) and (001) Catalysts. *JACS Au* **2021**, *1* (1), 41−52.

(5) Krüger, P.; Bourgeois, S.; Domenichini, B.; Magnan, H.; Chandesris, D.; Le Fevre, P.; Flank, A.; Jupille, J.; Floreano, L.; Cossaro, A.; et al. Defect States at the TiO_2 (110) Surface Probed by Resonant Photoelectron Diffraction. *Phys. Rev. Lett.* **2008**, *100* (5), 055501.

(6) Tsoukalou, A.; Abdala, P. M.; Stoian, D.; Huang, X.; Willinger, M. G.; Fedorov, A.; Muller, C. R. Structural Evolution and Dynamics of an In_2O_3 Catalyst for CO_2 Hydrogenation to Methanol: An Operando XAS-XRD and in Situ Tem Study. *J. Am. Chem. Soc.* **2019**, *141* (34), 13497−13505.

(7) Krüger, P.; Jupille, J.; Bourgeois, S.; Domenichini, B.; Verdini, A.; Floreano, L.; Morgante, A. Intrinsic Nature of the Excess Electron Distribution at the TiO_2 (110) Surface. *Phys. Rev. Lett.* **2012**, *108* (12), 126803.

(8) Lohaus, C.; Klein, A.; Jaegermann, W. Limitation of Fermi Level Shifts by Polaron Defect States in Hematite Photoelectrodes. *Nat. Commun.* **2018**, *9* (1), 4309.
(9) Wen, B.; Yin, W. J.; Selloni, A.; Liu, L. M. Defects, Adsorbates, and Photoactivity of Rutile TiO_2 (110): Insight by First-Principles Calculations. *J. Phys. Chem. Lett.* **2018**, *9* (18), 5281−5287.
(10) Reticcioli, M.; Sokolovic, I.; Schmid, M.; Diebold, U.; Setvin, M.; Franchini, C. Interplay between Adsorbates and Polarons: CO on Rutile TiO_2(110). *Phys. Rev. Lett.* **2019**, *122* (1), 016805.
(11) Carneiro, L. M.; Cushing, S. K.; Liu, C.; Su, Y.; Yang, P.; Alivisatos, A. P.; Leone, S. R. Excitation-Wavelength-Dependent Small Polaron Trapping of Photoexcited Carriers in Alpha-Fe_2O_3. *Nat. Mater.* **2017**, *16* (8), 819−825.
(12) Papageorgiou, A. C.; Beglitis, N. S.; Pang, C. L.; Teobaldi, G.; Cabailh, G.; Chen, Q.; Fisher, A. J.; Hofer, W. A.; Thornton, G. Electron Traps and Their Effect on the Surface Chemistry of TiO_2(110). *Proc. Natl. Acad. Sci. U. S. A.* **2010**, *107* (6), 2391−6.
(13) Chu, W.; Zheng, Q.; Prezhdo, O. V.; Zhao, J. CO_2 Photoreduction on Metal Oxide Surface Is Driven by Transient Capture of Hot Electrons: Ab Initio Quantum Dynamics Simulation. *J. Am. Chem. Soc.* **2020**, *142* (6), 3214−3221.
(14) Hirakawa, H.; Hashimoto, M.; Shiraishi, Y.; Hirai, T. Photocatalytic Conversion of Nitrogen to Ammonia with Water on Surface Oxygen Vacancies of Titanium Dioxide. *J. Am. Chem. Soc.* **2017**, *139* (31), 10929−10936.
(15) Rawool, S. A.; Yadav, K. K.; Polshettiwar, V. Defective TiO_2 for Photocatalytic CO_2 Conversion to Fuels and Chemicals. *Chem. Sci.* **2021**, *12* (12), 4267−4299.
(16) Kowalski, P. M.; Camellone, M. F.; Nair, N. N.; Meyer, B.; Marx, D. Charge Localization Dynamics Induced by Oxygen Vacancies on the TiO_2(110) Surface. *Phys. Rev. Lett.* **2010**, *105* (14), 146405.
(17) Hegner, F. S.; Forrer, D.; Galán-Mascarós, J. R.; López, N.; Selloni, A. Versatile Nature of Oxygen Vacancies in Bismuth Vanadate Bulk and (001) Surface. *J. Phys. Chem. Lett.* **2019**, *10* (21), 6672−6678.
(18) Setvin, M.; Franchini, C.; Hao, X.; Schmid, M.; Janotti, A.; Kaltak, M.; Van de Walle, C. G.; Kresse, G.; Diebold, U. Direct View at Excess Electrons in TiO_2 Rutile and Anatase. *Phys. Rev. Lett.* **2014**, *113* (8), 086402.
(19) Yim, C. M.; Watkins, M. B.; Wolf, M. J.; Pang, C. L.; Hermansson, K.; Thornton, G. Engineering Polarons at a Metal Oxide Surface. *Phys. Rev. Lett.* **2016**, *117* (11), 116402.
(20) Yang, S.; Brant, A. T.; Giles, N. C.; Halliburton, L. E. Intrinsic Small Polarons in Rutile TiO_2. *Phys. Rev. B* **2013**, *87* (12), 125201.
(21) Naldoni, A.; Allieta, M.; Santangelo, S.; Marelli, M.; Fabbri, F.; Cappelli, S.; Bianchi, C. L.; Psaro, R.; Dal Santo, V. Effect of Nature and Location of Defects on Bandgap Narrowing in Black TiO_2 Nanoparticles. *J. Am. Chem. Soc.* **2012**, *134* (18), 7600−3.
(22) Zuo, F.; Wang, L.; Wu, T.; Zhang, Z.; Borchardt, D.; Feng, P. Self-Doped Ti^{3+} Enhanced Photocatalyst for Hydrogen Production under Visible Light. *J. Am. Chem. Soc.* **2010**, *132* (34), 11856−11857.
(23) Corby, S.; Francas, L.; Selim, S.; Sachs, M.; Blackman, C.; Kafizas, A.; Durrant, J. R. Water Oxidation and Electron Extraction Kinetics in Nanostructured Tungsten Trioxide Photoanodes. *J. Am. Chem. Soc.* **2018**, *140* (47), 16168−16177.
(24) Selim, S.; et al. Impact of Oxygen Vacancy Occupancy on Charge Carrier Dynamics in $BiVO_4$ Photoanodes. *J. Am. Chem. Soc.* **2019**, *141* (47), 18791−18798.
(25) Zhao, Z.; Goncalves, R. V.; Barman, S. K.; Willard, E. J.; Byle, E.; Perry, R.; Wu, Z.; Huda, M. N.; Moulé, A. J.; Osterloh, F. E. Electronic Structure Basis for Enhanced Overall Water Splitting Photocatalysis with Aluminum Doped $SrTiO_3$ in Natural Sunlight. *Energy Environ. Sci.* **2019**, *12* (4), 1385−1395.
(26) Hulva, J.; Meier, M.; Bliem, R.; Jakub, Z.; Kraushofer, F.; Schmid, M.; Diebold, U.; Franchini, C.; Parkinson, G. S. Unraveling CO Adsorption on Model Single-Atom Catalysts. *Science* **2021**, *371* (6527), 375−379.
(27) Cao, Y.; Yu, M.; Qi, S.; Huang, S.; Wang, T.; Xu, M.; Hu, S.; Yan, S. Scenarios of Polaron-Involved Molecular Adsorption on Reduced TiO_2(110) Surfaces. *Sci. Rep.* **2017**, *7* (1), 6148.
(28) Tanner, A. J.; Wen, B.; Ontaneda, J.; Zhang, Y.; Grau-Crespo, R.; Fielding, H. H.; Selloni, A.; Thornton, G. Polaron-Adsorbate Coupling at the TiO_2(110)-Carboxylate Interface. *J. Phys. Chem. Lett.* **2021**, *12* (14), 3571−3576.
(29) Yim, C. M.; et al. Visualization of Water-Induced Surface Segregation of Polarons on Rutile TiO_2(110). *J. Phys. Chem. Lett.* **2018**, *9* (17), 4865−4871.
(30) Zhu, Y. N.; Teobaldi, G.; Liu, L. M. Water-Hydrogen-Polaron Coupling at Anatase TiO_2(101) Surfaces: A Hybrid Density Functional Theory Study. *J. Phys. Chem. Lett.* **2020**, *11* (11), 4317−4325.
(31) Barragan, A. A.; Hanukovich, S.; Bozhilov, K.; Yamijala, S.; Wong, B. M.; Christopher, P.; Mangolini, L. Photochemistry of Plasmonic Titanium Nitride Nanocrystals. *J. Phys. Chem. C* **2019**, *123* (35), 21796−21804.
(32) Zhao, Y.; Wang, Z.; Cui, X.; Huang, T.; Wang, B.; Luo, Y.; Yang, J.; Hou, J. What Are the Adsorption Sites for CO on the Reduced TiO_2(110)-1 × 1 Surface? *J. Am. Chem. Soc.* **2009**, *131* (23), 7958−7959.
(33) Yu, Y.-Y.; Gong, X.-Q. CO Oxidation at Rutile TiO_2(110): Role of Oxygen Vacancies and Titanium Interstitials. *ACS Catal.* **2015**, *5* (4), 2042−2050.
(34) Mu, R.; Dahal, A.; Wang, Z. T.; Dohnalek, Z.; Kimmel, G. A.; Petrik, N. G.; Lyubinetsky, I. Adsorption and Photodesorption of CO from Charged Point Defects on TiO_2(110). *J. Phys. Chem. Lett.* **2017**, *8* (18), 4565−4572.
(35) Xu, M.; Gao, Y.; Moreno, E. M.; Kunst, M.; Muhler, M.; Wang, Y.; Idriss, H.; Woll, C. Photocatalytic Activity of Bulk TiO_2 Anatase and Rutile Single Crystals Using Infrared Absorption Spectroscopy. *Phys. Rev. Lett.* **2011**, *106* (13), 138302.
(36) Reticcioli, M.; Diebold, U.; Kresse, G.; Franchini, C. Small Polarons in Transition Metal Oxides. *Handbook of Materials Modeling: Applications: Current and Emerging Materials* **2020**, 1035−1073.
(37) Akimov, A. V.; Prezhdo, O. V. Persistent Electronic Coherence Despite Rapid Loss of Electron−Nuclear Correlation. *J. Phys. Chem. Lett.* **2013**, *4* (22), 3857−3864.
(38) Akimov, A. V.; Prezhdo, O. V. Advanced Capabilities of the PYXAID Program: Integration Schemes, Decoherence Effects, Multiexcitonic States, and Field-Matter Interaction. *J. Chem. Theory Comput.* **2014**, *10* (2), 789−804.
(39) Craig, C. F.; Duncan, W. R.; Prezhdo, O. V. Trajectory Surface Hopping in the Time-Dependent Kohn-Sham Approach for Electron-Nuclear Dynamics. *Phys. Rev. Lett.* **2005**, *95* (16), 163001.
(40) Marques, M. A. L.; Gross, E. K. U. Time-Dependent Density Functional Theory. *Annu. Rev. Phys. Chem.* **2004**, *55* (1), 427−455.
(41) Runge, E.; Gross, E. K. U. Density-Functional Theory for Time-Dependent Systems. *Phys. Rev. Lett.* **1984**, *52* (12), 997−1000.
(42) Kresse, G.; Furthmüller, J. Efficient Iterative Schemes for Ab Initio Total-Energy Calculations Using a Plane-Wave Basis Set. *Phys. Rev. B* **1996**, *54* (16), 11169−11186.
(43) Perdew, J. P.; Burke, K.; Ernzerhof, M. Generalized Gradient Approximation Made Simple. *Phys. Rev. Lett.* **1996**, *77* (18), 3865−3868.
(44) Liechtenstein, A. I.; Anisimov, V. I.; Zaanen, J. Density-Functional Theory and Strong Interactions: Orbital Ordering in Mott-Hubbard Insulators. *Phys. Rev. B* **1995**, *52* (8), R5467−R5470.
(45) Morgan, B. J.; Watson, G. W. A DFT+U description of Oxygen Vacancies at the TiO_2 Rutile (110) Surface. *Surf. Sci.* **2007**, *601* (21), 5034−5041.
(46) Blöchl, P. E. Projector Augmented-Wave Method. *Phys. Rev. B* **1994**, *50* (24), 17953−17979.
(47) Heyd, J.; Scuseria, G. E.; Ernzerhof, M. Hybrid Functionals Based on a Screened Coulomb Potential. *J. Chem. Phys.* **2003**, *118* (18), 8207−8215.
(48) Liu, Z.-P.; Gong, X.-Q.; Kohanoff, J.; Sanchez, C.; Hu, P. Catalytic Role of Metal Oxides in Gold-Based Catalysts: A First

https://doi.org/10.1021/jacsau.1c00508
JACS Au 2022, 2, 234−245

Principles Study of CO Oxidation on Tio_2 Supported Au. *Phys. Rev. Lett.* **2003**, *91* (26), 266102.
(49) Liu, L. M.; McAllister, B.; Ye, H. Q.; Hu, P. Identifying an O_2 Supply Pathway in CO Oxidation on Au/TiO_2(110): A Density Functional Theory Study on the Intrinsic Role of Water. *J. Am. Chem. Soc.* **2006**, *128* (12), 4017−4022.
(50) Di Valentin, C.; Pacchioni, G.; Selloni, A. Electronic Structure of Defect Dtates in Hydroxylated and Reduced Rutile TiO_2(110) Surfaces. *Phys. Rev. Lett.* **2006**, *97* (16), 166803.
(51) Guo, C.; et al. Probing Nonequilibrium Dynamics of Photoexcited Polarons on a Metal-Oxide Surface with Atomic Precision. *Phys. Rev. Lett.* **2020**, *124* (20), 206801.
(52) Xie, X.-Y.; Xiao, P.; Fang, W.-H.; Cui, G.; Thiel, W. Probing Photocatalytic Nitrogen Reduction to Ammonia with Water on the Rutile TiO_2(110) Surface by First-Principles Calculations. *ACS Catal.* **2019**, *9* (10), 9178−9187.
(53) Grimme, S.; Antony, J.; Ehrlich, S.; Krieg, H. A Consistent and Accurate Ab Initio Parametrization of Density Functional Dispersion Correction (DFT-D) for the 94 Elements H-Pu. *J. Chem. Phys.* **2010**, *132* (15), 154104.
(54) Grimme, S.; Ehrlich, S.; Goerigk, L. Effect of the Damping Function in Dispersion Corrected Density Functional Theory. *J. Comput. Chem.* **2011**, *32* (7), 1456−1465.
(55) Jaeger, H. M.; Fischer, S.; Prezhdo, O. V. Decoherence-Induced Surface Hopping. *J. Chem. Phys.* **2012**, *137* (22), 22A545.
(56) Fischer, S. A.; Habenicht, B. F.; Madrid, A. B.; Duncan, W. R.; Prezhdo, O. V. Regarding the Validity of the Time-Dependent Kohn-Sham Approach for Electron-Nuclear Dynamics Via Trajectory Surface Hopping. *J. Chem. Phys.* **2011**, *134* (2), 024102.
(57) Akimov, A. V. A Simple Phase Correction Makes a Big Difference in Nonadiabatic Molecular Dynamics. *J. Phys. Chem. Lett.* **2018**, *9* (20), 6096−6102.
(58) Chu, W.; Prezhdo, O. V. Concentric Approximation for Fast and Accurate Numerical Evaluation of Nonadiabatic Coupling with Projector Augmented-Wave Pseudopotentials. *J. Phys. Chem. Lett.* **2021**, *12* (12), 3082−3089.
(59) Chu, W.; Zheng, Q.; Akimov, A. V.; Zhao, J.; Saidi, W. A.; Prezhdo, O. V. Accurate Computation of Nonadiabatic Coupling with Projector Augmented-Wave Pseudopotentials. *J. Phys. Chem. Lett.* **2020**, *11* (23), 10073−10080.
(60) Kilina, S. V.; Neukirch, A. J.; Habenicht, B. F.; Kilin, D. S.; Prezhdo, O. V. Quantum Zeno Effect Rationalizes the Phonon Bottleneck in Semiconductor Quantum Dots. *Phys. Rev. Lett.* **2013**, *110* (18), 180404.
(61) Englman, R.; Jortner, J. The Energy Gap Law for Non-Radiative Decay in Large Molecules. *J. Lumin.* **1970**, *1*−*2*, 134−142.
(62) Long, R.; Casanova, D.; Fang, W.-H.; Prezhdo, O. V. Donor−Acceptor Interaction Determines the Mechanism of Photoinduced Electron Injection from Graphene Quantum Dots into TiO_2: Π-Stacking Supersedes Covalent Bonding. *J. Am. Chem. Soc.* **2017**, *139* (7), 2619−2629.
(63) Long, R.; English, N. J.; Prezhdo, O. V. Photo-Induced Charge Separation across the Graphene-TiO_2 Interface Is Faster Than Energy Losses: A Time-Domain Ab Initio Analysis. *J. Am. Chem. Soc.* **2012**, *134* (34), 14238−48.
(64) Long, R.; Prezhdo, O. V. Instantaneous Generation of Charge-Separated State on TiO_2 Surface Sensitized with Plasmonic Nanoparticles. *J. Am. Chem. Soc.* **2014**, *136* (11), 4343−54.
(65) Zhou, Z.; Liu, J.; Long, R.; Li, L.; Guo, L.; Prezhdo, O. V. Control of Charge Carriers Trapping and Relaxation in Hematite by Oxygen Vacancy Charge: Ab Initio Non-Adiabatic Molecular Dynamics. *J. Am. Chem. Soc.* **2017**, *139* (19), 6707−6717.
(66) Cheng, C.; Fang, Q.; Fernandez-Alberti, S.; Long, R. Controlling Charge Carrier Trapping and Recombination in $BiVO_4$ with the Oxygen Vacancy Oxidation State. *J. Phys. Chem. Lett.* **2021**, *12* (14), 3514−3521.
(67) Zhang, L.; Zheng, Q.; Xie, Y.; Lan, Z.; Prezhdo, O. V.; Saidi, W. A.; Zhao, J. Delocalized Impurity Phonon Induced Electron-Hole Recombination in Doped Semiconductors. *Nano Lett.* **2018**, *18* (3), 1592−1599.
(68) Li, L.; Long, R.; Bertolini, T.; Prezhdo, O. V. Sulfur Adatom and Vacancy Accelerate Charge Recombination in MoS_2 but by Different Mechanisms: Time-Domain Ab Initio Analysis. *Nano Lett.* **2017**, *17* (12), 7962−7967.
(69) Li, L.; Long, R.; Prezhdo, O. V. Charge Separation and Recombination in Two-Dimensional MoS_2/WS_2: Time-Domain Ab Initio Modeling. *Chem. Mater.* **2017**, *29* (6), 2466−2473.
(70) Wang, X.; Long, R. Oxidation Notably Accelerates Non-radiative Electron-Hole Recombination in MoS_2 by Different Mechanisms: Time-Domain Ab Initio Analysis. *J. Phys. Chem. Lett.* **2020**, *11*, 4086−4092.
(71) Wei, Y.; Li, L.; Fang, W.; Long, R.; Prezhdo, O. V. Weak Donor-Acceptor Interaction and Interface Polarization Define Photo-excitation Dynamics in the MoS_2/TiO_2 Composite: Time-Domain Ab Initio Simulation. *Nano Lett.* **2017**, *17* (7), 4038−4046.
(72) Zhang, Z.; Liu, L.; Fang, W.-H.; Long, R.; Tokina, M. V.; Prezhdo, O. V. Plasmon-Mediated Electron Injection from Au Nanorods into MoS_2: Traditional Versus Photoexcitation Mechanism. *Chem.* **2018**, *4* (5), 1112−1127.
(73) Lu, H.; Wei, Y.; Long, R. Charge Localization Induced by Nanopore Defects in Monolayer Black Phosphorus for Suppressing Nonradiative Electron-Hole Recombination through Time-Domain Simulation. *Acta Phys. -Chim. Sin.* **2022**, *37*, 2006064.
(74) He, J.; Fang, W. H.; Long, R.; Prezhdo, O. V. Superoxide/Peroxide Chemistry Extends Charge Carriers' Lifetime but Undermines Chemical Stability of $CH_3NH_3PbI_3$ Exposed to Oxygen: Time-Domain Ab Initio Analysis. *J. Am. Chem. Soc.* **2019**, *141* (14), 5798−5807.
(75) Qiao, L.; Fang, W. H.; Long, R.; Prezhdo, O. V. Extending Carrier Lifetimes in Lead Halide Perovskites with Alkali Metals by Passivating and Eliminating Halide Interstitial Defects. *Angew. Chem., Int. Ed. Engl.* **2020**, *59* (12), 4684−4690.
(76) Qiao, L.; Fang, W.-H.; Long, R. The Interplay between Lead Vacancy and Water Rationalizes the Puzzle of Charge Carrier Lifetimes in $CH_3NH_3PbI_3$: Time-Domain Ab Initio Analysis. *Angew. Chem., Int. Ed.* **2020**, *59* (32), 13347−13353.
(77) Qiao, L.; Fang, W.-H.; Long, R.; Prezhdo, O. V. Photoinduced Dynamics of Charge Carriers in Metal Halide Perovskites from an Atomistic Perspective. *J. Phys. Chem. Lett.* **2020**, *11* (17), 7066−7082.
(78) Ye, S.; Ding, C.; Chen, R.; Fan, F.; Fu, P.; Yin, H.; Wang, X.; Wang, Z.; Du, P.; Li, C. Mimicking the Key Functions of Photosystem II in Artificial Photosynthesis for Photoelectrocatalytic Water Splitting. *J. Am. Chem. Soc.* **2018**, *140* (9), 3250−3256.
(79) Li, W.; She, Y.; Vasenko, A. S.; Prezhdo, O. V. Ab Initio Nonadiabatic Molecular Dynamics of Charge Carriers in Metal Halide Perovskites. *Nanoscale* **2021**, *13*, 10239−10265.
(80) Chaban, V. V.; Prezhdo, V. V.; Prezhdo, O. V. Covalent Linking Greatly Enhances Photoinduced Electron Transfer in Fullerene-Quantum Dot Nanocomposites: Time-Domain Ab Initio Study. *J. Phys. Chem. Lett.* **2013**, *4* (1), 1−6.
(81) Chu, W.; Saidi, W. A.; Zheng, Q.; Xie, Y.; Lan, Z.; Prezhdo, O. V.; Petek, H.; Zhao, J. Ultrafast Dynamics of Photongenerated Holes at a CH_3OH/TiO_2 Rutile Interface. *J. Am. Chem. Soc.* **2016**, *138* (41), 13740−13749.
(82) Akimov, A. V.; Asahi, R.; Jinnouchi, R.; Prezhdo, O. V. What Makes the Photocatalytic CO_2 Reduction on N-Doped Ta_2O_5 Efficient: Insights from Nonadiabatic Molecular Dynamics. *J. Am. Chem. Soc.* **2015**, *137* (35), 11517−11525.
(83) Wang, L.; Prezhdo, O. V.; Beljonne, D. Mixed Quantum-Classical Dynamics for Charge Transport in Organics. *Phys. Chem. Chem. Phys.* **2015**, *17* (19), 12395−406.
(84) Parandekar, P. V.; Tully, J. C. Mixed Quantum-Classical Equilibrium. *J. Chem. Phys.* **2005**, *122* (9), 094102.
(85) Momma, K.; Izumi, F. VESTA 3 for Three-Dimensional Visualization of Crystal, Volumetric and Morphology Data. *J. Appl. Crystallogr.* **2011**, *44* (6), 1272−1276.

https://doi.org/10.1021/jacsau.1c00508
JACS Au 2022, 2, 234−245

(86) Shibuya, T.; Yasuoka, K.; Mirbt, S.; Sanyal, B. A Systematic Study of Polarons Due to Oxygen Vacancy Formation at the Rutile TiO2(110) Surface by GGA + U and HSE06 Methods. *J. Phys.: Condens. Matter* **2012**, *24* (43), 435504.
(87) Cai, Y.; Bai, Z.; Chintalapati, S.; Zeng, Q.; Feng, Y. P. Transition Metal Atoms Pathways on Rutile TiO_2(110) Surface: Distribution of Ti^{3+} States and Evidence of Enhanced Peripheral Charge Accumulation. *J. Chem. Phys.* **2013**, *138* (15), 154711.
(88) Esch, T. R.; Bredow, T. Band Positions of Rutile Surfaces and the Possibility of Water Splitting. *Surf. Sci.* **2017**, *665*, 20−27.
(89) Wen, B.; Hao, Q.; Yin, W.-J.; Zhang, L.; Wang, Z.; Wang, T.; Zhou, C.; Selloni, A.; Yang, X.; Liu, L.-M. Electronic Structure and Photoabsorption of Ti^{3+} Ions in Reduced Anatase and Rutile TiO_2. *Phys. Chem. Chem. Phys.* **2018**, *20* (26), 17658−17665.
(90) Basiuk, V. A.; Prezhdo, O. V.; Basiuk, E. V. Thermal Smearing in DFT Calculations: How Small Is Really Small? A Case of La and Lu Atoms Adsorbed on Graphene. *Mater. Today Commun.* **2020**, *25*, 101595.
(91) Reticcioli, M.; Setvin, M.; Schmid, M.; Diebold, U.; Franchini, C. Formation and Dynamics of Small Polarons on the Rutile TiO_2(110) Surface. *Phys. Rev. B* **2018**, *98* (4), 045306.
(92) Wagstaffe, M.; Noei, H.; Stierle, A. Elucidating the Defect-Induced Changes in the Photocatalytic Activity of TiO_2. *J. Phys. Chem. C* **2020**, *124* (23), 12539−12547.
(93) Yin, H.; Wada, Y.; Kitamura, T.; Kambe, S.; Murasawa, S.; Mori, H.; Sakata, T.; Yanagida, S. Hydrothermal Synthesis of Nanosized Anatase and Rutile TiO_2 Using Amorphous Phase TiO_2. *J. Mater. Chem.* **2001**, *11* (6), 1694−1703.
(94) Estreicher, S.; Gibbons, T.; Kang, B.; Bebek, M. Phonons and Defects in Semiconductors and Nanostructures: Phonon Trapping, Phonon Scattering, and Heat Flow at Heterojunctions. *J. Appl. Phys.* **2014**, *115* (1), 012012.
(95) Akemann, W.; Otto, A. Vibrational Modes of CO Adsorbed on Disordered Copper Films. *J. Raman Spectrosc.* **1991**, *22* (12), 797−803.
(96) Cheng, C.; Fang, W.-H.; Long, R.; Prezhdo, O. V. Water Splitting with a Single-Atom Cu/TiO_2 Photocatalyst: Atomistic Origin of High Efficiency and Proposed Enhancement by Spin Selection. *JACS Au* **2021**, *1* (5), 550−559.
(97) Wei, Y.; Tokina, M. V.; Benderskii, A. V.; Zhou, Z.; Long, R.; Prezhdo, O. V. Quantum Dynamics Origin of High Photocatalytic Activity of Mixed-Phase Anatase/Rutile TiO_2. *J. Chem. Phys.* **2020**, *153* (4), 044706.
(98) Mukamel, S. *Principles of Nonlinear Optical Spectroscopy*; Oxford University Press: New York, 1995.
(99) Yamada, Y.; Kanemitsu, Y. Determination of Eectron and Hole Lifetimes of Rutile and Anatase TiO_2 Single Crystals. *Appl. Phys. Lett.* **2012**, *101* (13), 133907.
(100) Wei, Y.; Zhou, Z.; Fang, W. H.; Long, R. Grain Boundary Facilitates Photocatalytic Reaction in Rutile TiO_2 Despite Fast Charge Recombination: A Time-Domain Ab Initio Analysis. *J. Phys. Chem. Lett.* **2018**, *9* (19), 5884−5889.

https://doi.org/10.1021/jacsau.1c00508
JACS Au 2022, 2, 234−245